Electronic Supplementary Information

Rate-independent and ultra-stable low-temperature sodium storage in pseudocapacitive TiO_2 nanowires

Dongmei Lin,‡[a] Kaikai Li,‡[a] Qian Wang,[a] Linlong Lyu,[a] Baohua Li*[b] and Limin Zhou*[a]

[a] Department of Mechanical Engineering, The Hong Kong Polytechnic University, Hong Kong, China.
[b] Engineering Laboratory for the Next Generation Power and Energy Storage Batteries, Graduate School at Shenzhen, Tsinghua University, Shenzhen 518055, China.

Corresponding Authors

*E-mail: mmlmzhou@polyu.edu.hk (Prof. Limin Zhou)
*E-mail: libh@sz.tsinghua.edu.cn (Prof. Baohua Li)

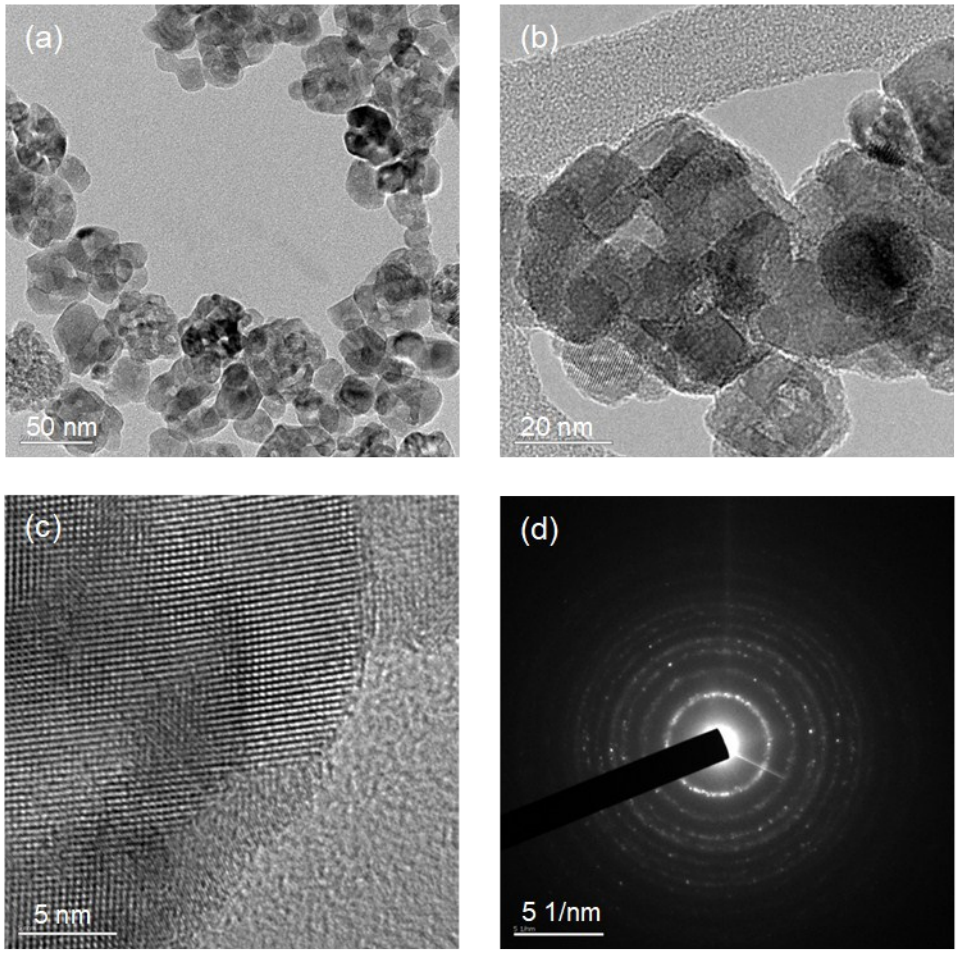

Fig. S1 (a-b) TEM images of the precursor TiO_2 nanoparticles. (c) HRTEM image of the precursor TiO_2 nanoparticle. (d) SAED pattern of the precursor TiO_2 nanoparticles.

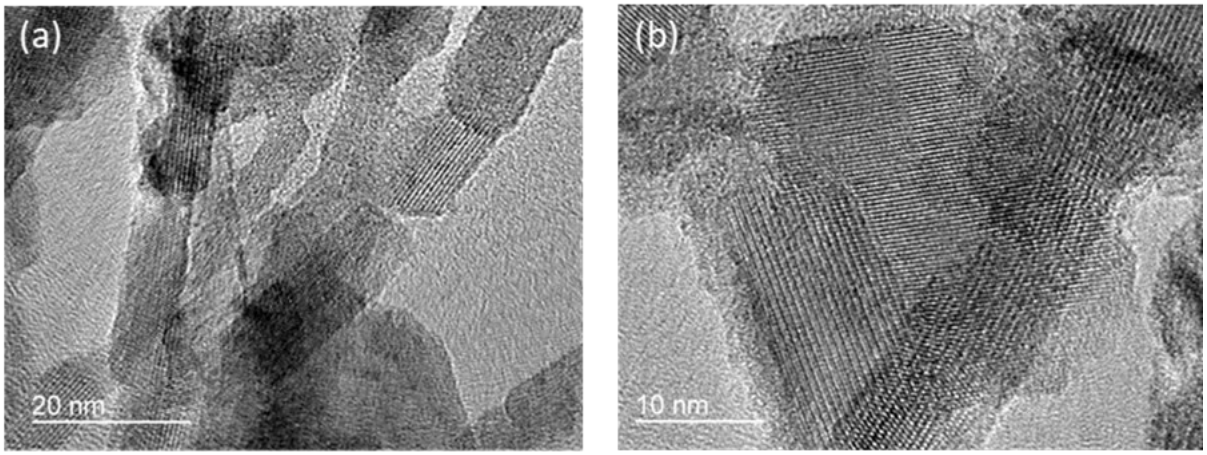

Fig. S2 HRTEM images of dual-phase TiO_2 nanowires.

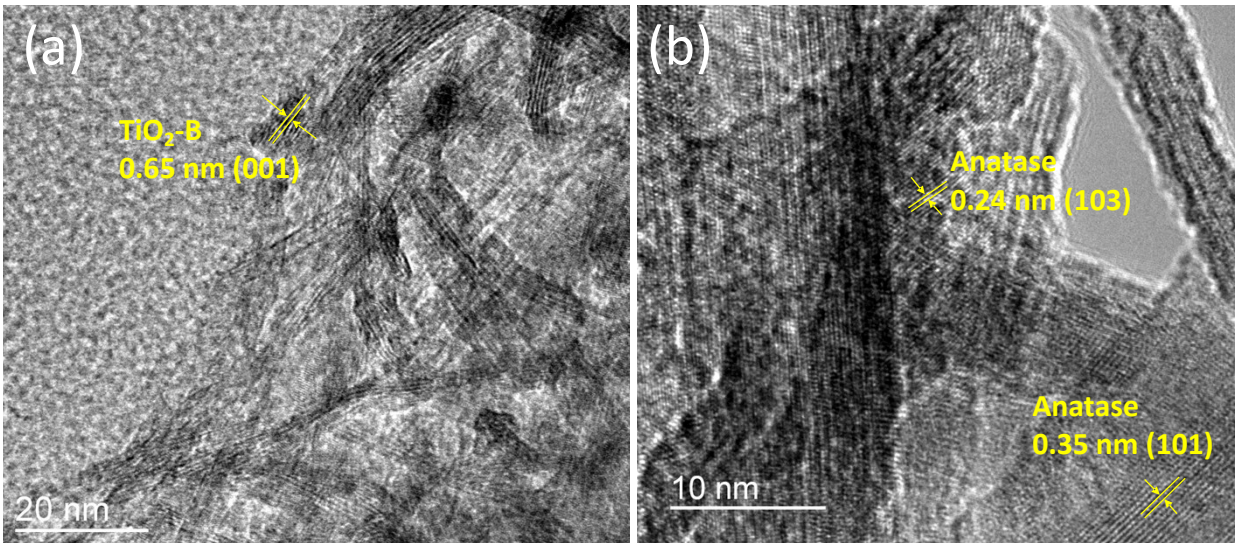

Fig. S3 HRTEM images of (a) pure TiO_2-B and (b) pure anatase nanowires.

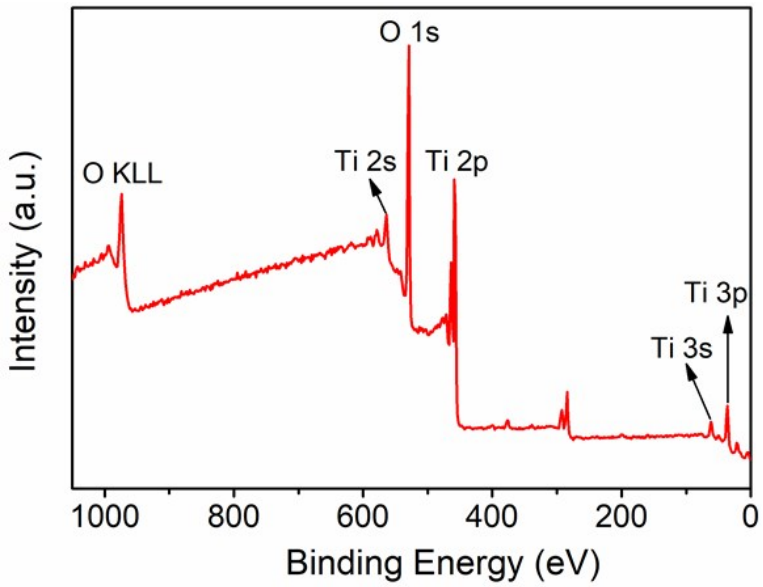

Fig. S4 XPS spectrum of the dual-phase TiO_2 nanowires.

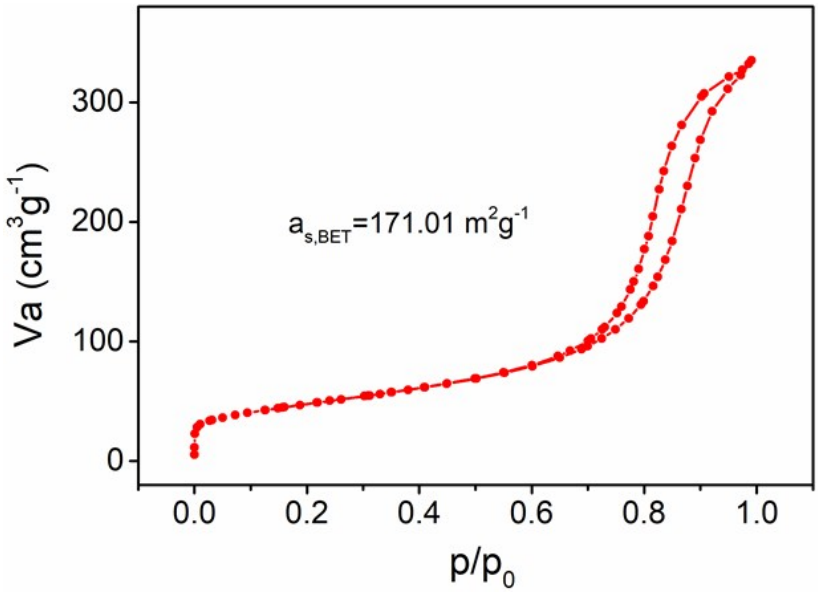

Fig. S5 Nitrogen adsorption/desorption isotherm of the dual-phase TiO_2 nanowires.

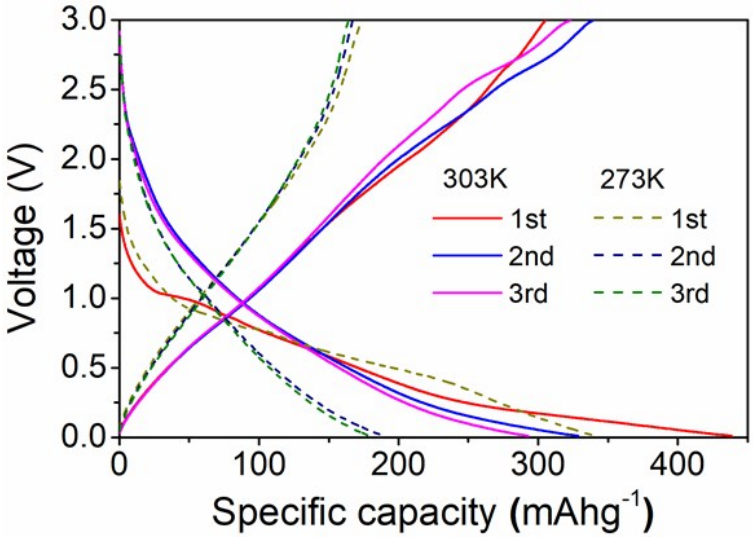

Fig. S6 The first three charge–discharge voltage profiles at a rate of 0.25 C (1 C = 335 mA g^{-1}) between 0.01 V and 3 V at 303 K and 273 K.

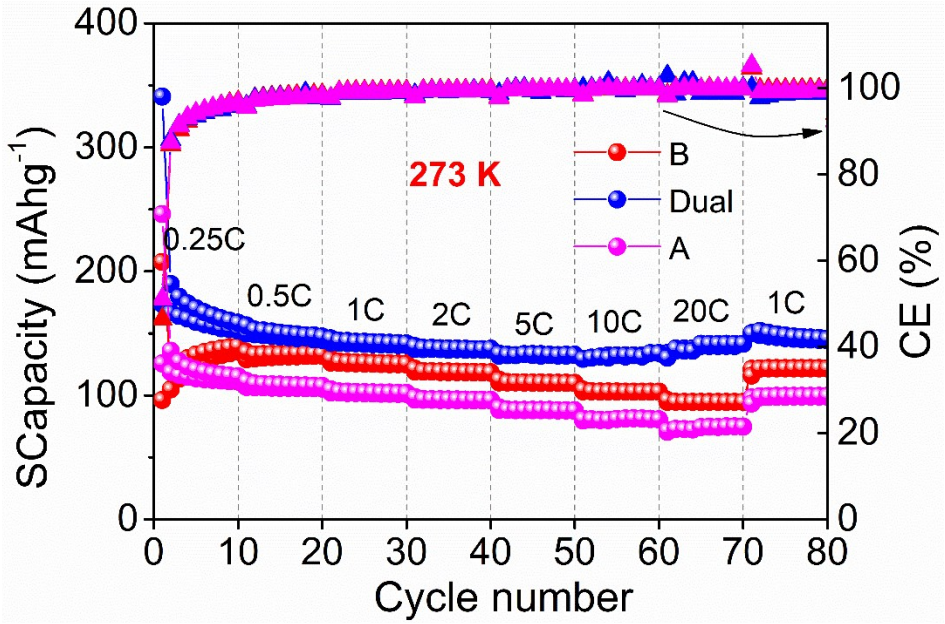

Fig. S7 Comparison of the rate-performance of the TiO_2 nanowires with different phases at 273 K.

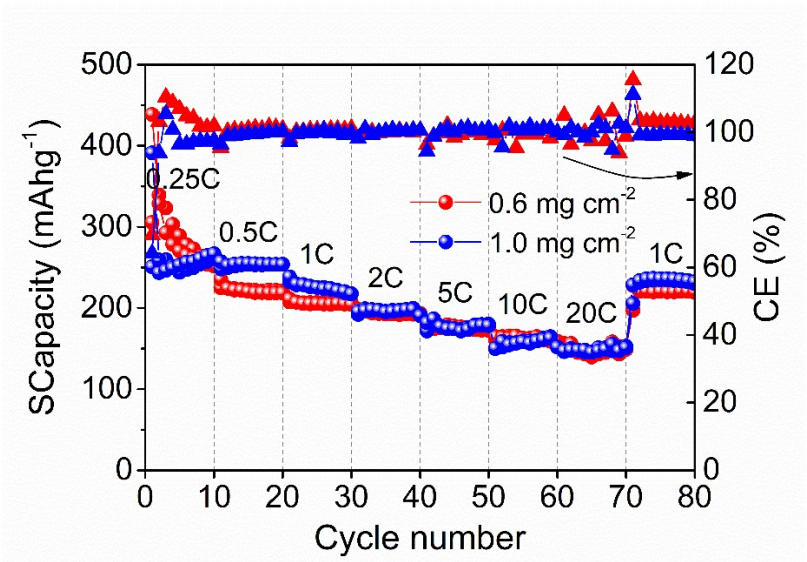

Fig. S8 Comparison of the rate-performance of the dual-phase TiO_2 nanowire electrodes with different mass loadings.

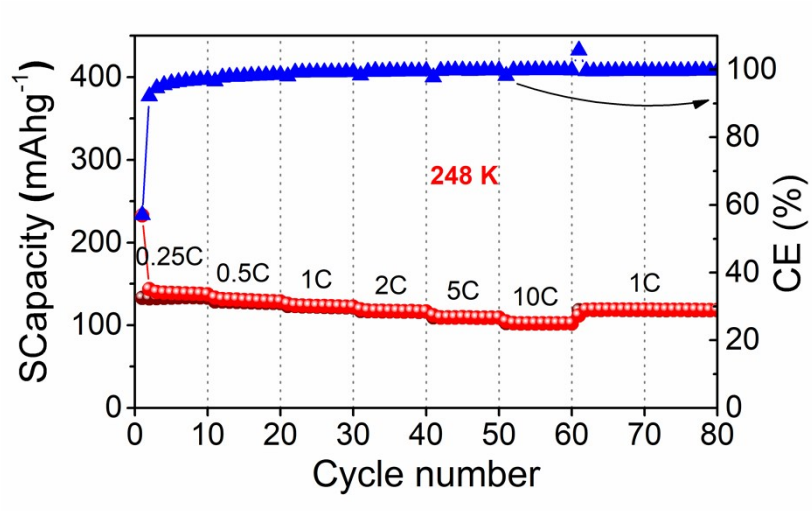

Fig. S9 Rate-performance of the dual-phase TiO_2 nanowires at 248 K.

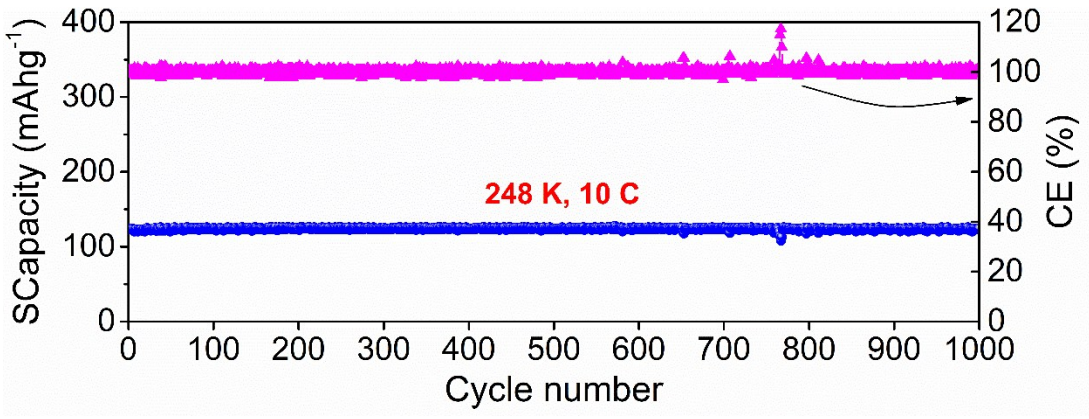

Fig. S10 Cycling performance of the dual-phase TiO_2 nanowire anode at a rate of 10 C for 1000 cycles at 248 K.

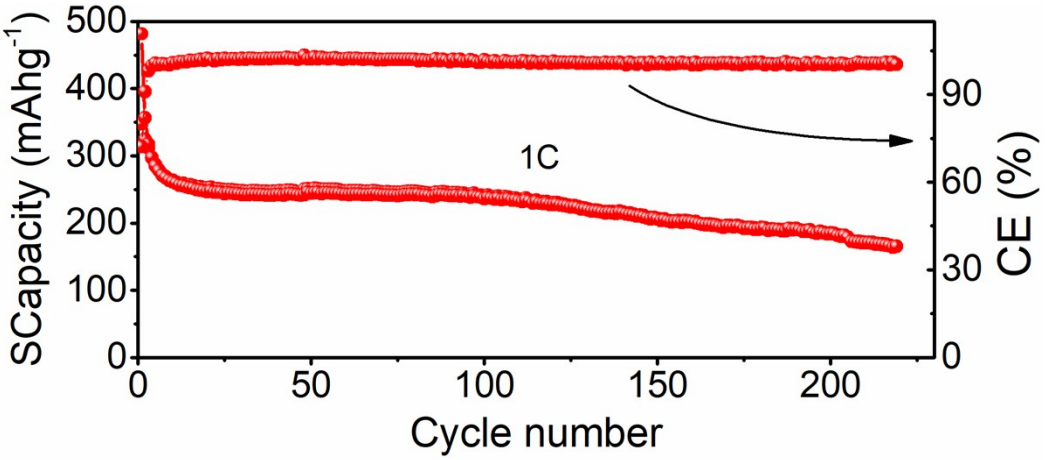

Fig. S11 Cycling performance of the dual-phase TiO_2 nanowire anode at a rate of 1 C for more than 200 cycles at 303 K.

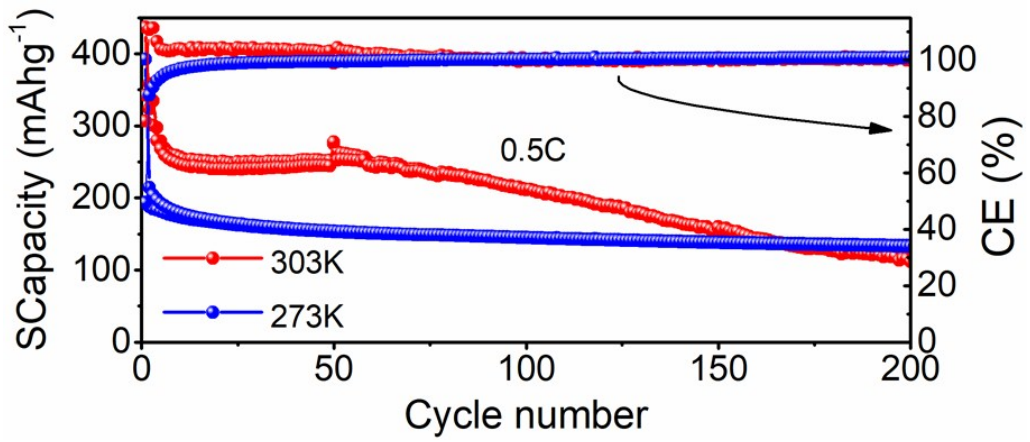

Fig. S12 Cycling performance of the dual-phase TiO_2 nanowire anode at a rate of 0.5 C for 200 cycles at 303 K and 273 K.

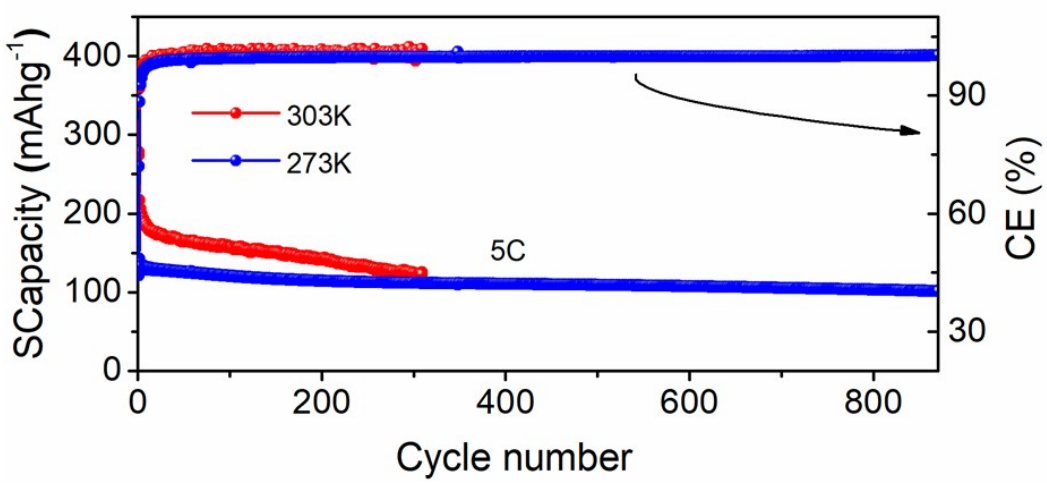

Fig. S13 Cycling performance at rate of 5 C at 303 K and 273 K.

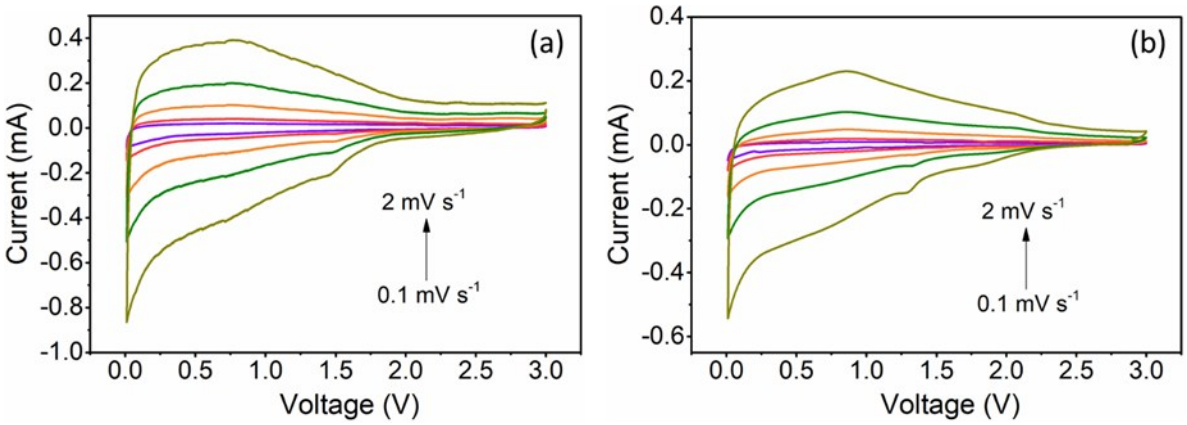

Fig. S14 Cyclic Voltammetry (CV) of the dual-phase TiO_2 nanowire anode at various scan rates from 0.1 to 20 mV s^{-1} at (a) 303 K and (b) 273 K.

Table S1. Comparison of the initial coulombic efficiency (ICE) of different TiO_2–based anode materials for SIBs reported in literatures at room temperature.

TiO_2–based anode materials	ICE (%)	Ref
TiO_2@NFG HPHNSs	49	1
a-TiO_2-x/r-TiO_2-x	40	2
C-TiO_2 (15 nm)	32.6	3
C-TiO_2 (11 nm)	38.2	3
pure TiO_2	59.4	4
boron doping TiO_2	62.5	4
anatase TiO_2 nanoparticles	42	5
anatase TiO_2 nanorods	<30	6
anatase TiO_2 nanocrystals	41.9	7
dual-phase TiO_2 nanowires	**69.6**	**this work**

Table S2. Comparison of the charge transfer resistance of different TiO_2–based anode materials for SIBs reported in literatures at room temperature.

TiO_2–based anode materials	**Charge transfer resistance R_{ct} (Ω)**	**Ref**
Nanocrystalline TiO_2(B)	73	8
mesoporous TiO_2 nanofibers	188	9
$NaTi_2(PO_4)_3$-Rutile TiO_2	74.0	10
anatase TiO_2 nanocrystal	108.7	11
Anatase@TiO_2(B) bicrystalline	75	12
Boron-doped TiO_2	310	4
N-TiO_2/C-dots composite	152	13
Sn-doped TiO_2 nanotubes	162.4	14
dual-phase TiO_2 nanowires	**4.95**	**this work**

Table S3. Charge transfer resistance of the dual-phase TiO_2 nanowire anode for SIBs at different temperatures.

Temperature	Charge transfer resistance Rct (Ω)
0	5.81
10	5.6
20	4.95
30	4.68
40	4.51
50	4.09

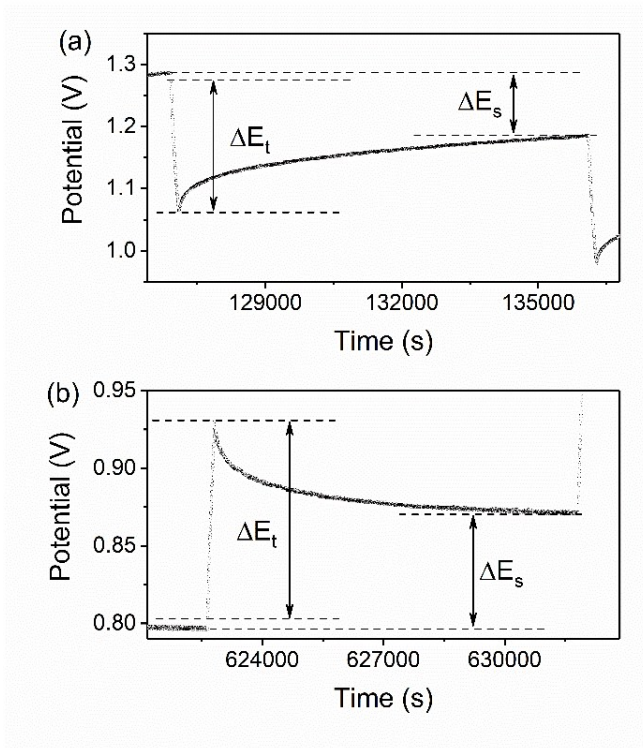

Fig. S15 Voltage profile for a single titration of the GITT (a) discharge and (b) charge.

The apparent Na^+ diffusion coefficients D_{app} were calculated using the following equation,[15] by assuming that Na^+ transport in the electrode obeys Fick's second law:

$$D_{app} = \frac{4}{\pi\tau}\left(\frac{m_B V_M}{M_B S}\right)^2 \left(\frac{\Delta E_s}{\Delta E_t}\right)^2$$

where τ is current pulse time, m_B, V_M and M_B are the mass, molar volume and atomic weight of the electrode material TiO_2, S is the area of the electrode.

GITT measurements consisting of a series of current pulses were applied to the pouch cell at a current density of 0.5 C (1 C = 335 mA g^{-1}) for 3 min, each followed by a 150 min relaxation period. The relaxation time of 150 min was selected to allow full relaxation of the open-circuit potential (OCP), and to minimize the self-discharge during the test. The voltage window of GITT measurement was 0.01 V to 3 V. Prior to the GITT measurement, the cell was galvanostatic cycled at 0.5 C for 5 cycles between 0.01 V to 3 V.

References

1 B. Li, B. Xi, Z. Feng, Y. Lin, J. Liu, J. Feng, Y. Qian and S. Xiong, *Adv. Mater.*, 2018, **30**, 1705788.

2 Y. Wu, Y. Jiang, J. Shi, L. Gu and Y. Yu, *Small*, 2017, **13**, 1700129.

3 M. N. Tahir, B. Oschmann, D. Buchholz, X. Dou, I. Lieberwirth, M. Panthöfer, W. Tremel, R. Zentel and S. Passerini, *Adv. Energy Mater.*, 2016, **6**, 1501489.

4 B. Wang, F. Zhao, G. Du, S. Porter, Y. Liu, P. Zhang, Z. Cheng, H.K. Liu and Z. Huang, *ACS Appl. Mater. Interfaces*, 2016, **8**, 16009-16015.

5 L. Wu, D. Buchholz, D. Bresser, L. Gomes Chagas and S. Passerini, *J. Power Sources*, 2014, **251**, 379-385.

6 K.-T. Kim, G. Ali, K.Y. Chung, C.S. Yoon, H. Yashiro, Y.-K. Sun, J. Lu, K. Amine and S.-T. Myung, *Nano Lett.*, 2014, **14**, 416-422.

7 Y. Xu, E.M. Lotfabad, H. Wang, B. Farbod, Z. Xu, A. Kohandehghan and D. Mitlin, *Chem. Commun.*, 2013, **49**, 8973-8975.

8 L. Wu, D. Bresser, D. Buchholz and S. Passerini, *J. Electrochem. Soc.*, 2015, **162**, A3052-A3058.

9 Y. Wu, X. Liu, Z. Yang, L. Gu and Y. Yu, *Small*, 2016, **12**, 3522-3529.

10 J. Yang, H. Wang, P. Hu, J. Qi, L. Guo and L. Wang, *Small*, 2015, **11**, 3744-3749.

11 Y. Xu, E.M. Lotfabad, H. Wang, B. Farbod, Z. Xu, A. Kohandehghan and D. Mitlin, *Chem. Commun.*, 2013, **49**, 8973-8975.

12 Z. Yan, L. Liu, J. Tan, Q. Zhou, Z. Huang, D. Xia, H. Shu, X. Yang and X. Wang, *J. Power Sources*, 2014, **269**, 37-45.

13 Y. Yang, X. Ji, M. Jing, H. Hou, Y. Zhu, L. Fang, X. Yang, Q. Chen and C.E. Banks, *J. Mater. Chem. A*, 2015, **3**, 5648-5655.

14 D. Yan, C. Yu, Y. Bai, W. Zhang, T. Chen, B. Hu, Z. Sun and L. Pan, *Chem. Commun.*, 2015, **51**, 8261-8264.

15 W. Weppner and R. A. Huggins, *J. Electrochem. Soc.*, 1977, **124**, 1569-1578.